Aerotecnica Missili & Spazio

Venus-Centered Heliosynchronous Orbits with Smart Dusts

Marco Bassetto · Giovanni Mengali · Alessandro A. Quarta

December 2019, Volume 98, Issue 4, pp. 301–308 https://doi.org/10.1007/s42496-019-00027-0

Abstract This paper deals with the problem of determining an analytical control law capable of maintaining highly-elliptical heliosynchronous polar orbits around Venus. The problem is addressed using the Smart Dust concept, a propellantless propulsion system that extracts momentum from the solar rays using a reflective coating. The modulation of the thrust magnitude is performed by exploiting the property of electrochromic materials of changing their optical characteristics through the application of an electrical voltage. The propulsive acceleration can therefore be switched from a minimum to a maximum value (o vice versa) so as to obtain a simple on-off control law. The required Smart Dust performance are described in closed form as a function of the semimajor axis and eccentricity of the working orbit. The soundness of the analytical control law is validated through a numerical integration of the equations of motion, in which the orbital perturbations due to the oblateness of Venus and to the gravitational attraction of the Sun are also included.

Keywords Smart Dust · Heliosynchronous orbits · Taranis orbits · polar orbits · Venus

1. Introduction

This paper investigates the possibility of generating nearly polar heliosynchronous eccentric orbits around Venus. A heliosynchronous orbit is characterized by a precession of the node line equal to the mean motion of the planet around the Sun [1]. Although the planet oblateness usually induces a secular variation of the right ascension of the ascending node when the orbit is nearly polar [2], such a precession may be insufficient and, therefore, a propulsion system is necessary to achieve the desired precession rate. To that end, Macdonald et al. [3] considered the extension of heliosynchronous orbits around the Earth using a non-orientation-constrained low-thrust propulsion system. In particular, Ref. [3] provides an analytical control law capable of guaranteeing the free selection of both orbit altitude and inclination. Docherty and Macdonald [4] investigated the analytical solution of low-thrust transfer trajectories between heliosynchronous orbits. Moreover, Anderson and Macdonald [1] developed heliosynchronous and highly elliptical orbits, in which the required thrust magnitude is given as a function of the local perturbations acting on the spacecraft. Finally, Wu et al. [5] developed heliosynchronous orbits around terrestrial planets using solar electric propulsion for the exploration of planet surface and atmosphere.

M. Bassetto (**corresponding author**)
University of Pisa
Tel.: +39 050 2217222
Fax.: +39 050 2217244
E-mail: marco.bassetto@ing.unipi.it

G. Mengali
University of Pisa
E-mail: g.mengali@ing.unipi.it

A. A. Quarta
University of Pisa
E-mail: a.quarta@ing.unipi.it

In this paper, heliosynchronous orbits are generated using Smart Dusts (SDs) [6,7], which exploit the solar radiation pressure to create a propulsive acceleration. The solar radiation pressure may significantly modify the SD orbit thanks to the high value of its area-to-mass ratio [8]. In the context of heliosynchronous orbits generated by photon-propelled spaceships, Tscherbakova et al. [9] dealt with the problem of stabilizing heliosynchronous orbits around the Earth using a balloon satellite under the effect of the light pressure of solar rays, whereas Cao et al. [10] proposed to use a femtosatellite swarm in heliosynchronous orbit for Earth remote sensing by taking advantage of solar radiation pressure for orbit control.

The collection of atmospheric data around Venus is a necessary step for understanding why Earth and Venus undergone two completely different evolutions despite their common geophysical characteristics [11]. This is possible by means of heliosynchronous polar orbits around Venus. The aim of this paper is therefore to determine an on-off control law that ensures a precession rate of the node line equal to the mean motion of Venus, while keeping both the argument of periapsis and the orbital inclination constant. These trajectories belong to the set of the so-called Taranis orbits [1], which are also characterized by high eccentricity and constant argument of periapsis. A Taranis orbit is typically generated by exploiting low-thrust propulsion systems to offset the drift of the apse line caused by the oblateness of the planet [12,13,14]. To that end, electrochromic coating systems may be used to exploit the peculiarity of electrochromic materials of changing their optical properties through the application of an electrical voltage [15]. In fact, SDs are capable of generating two values of propulsive acceleration thanks to the coverage of their surface by means of electrochromic material [16,17,18]. This paper shows that the required propulsive acceleration can be expressed in closed form as a function of both the semimajor axis and eccentricity of the SD reference orbit. In particular, the required performance increases for smaller values of semimajor axis and eccentricity. The soundness of the analytical control law is confirmed by numerical integration, in which the third-body perturbation due to the Sun and the gravitational field of Venus up to the J_4 zonal harmonic are also taken into account.

The paper is organized as follows. Sections 2 describes the mathematical model (that is, the differential equations that govern the SD motion) and derives the analytical control law for maintaining heliosynchronous Taranis orbits around Venus. Section 3 deals with a case study, and shows some numerical simulations that are useful to validate the soundness of the analytical control law. Finally, Section 4 contains some concluding remarks.

2. Mathematical model

The control law for creating heliosynchronous Taranis orbits is obtained in closed form by neglecting the perturbative accelerations due to Venus' oblateness and to the third-body perturbation of the Sun, and assuming the propulsive acceleration given by the solar radiation pressure to be oriented perpendicularly to the osculating orbital plane of the spacecraft. The latter assumption is reasonable when the SD orbital plane is orthogonal to the Sun-Venus line, and the SD is able to passively maintain a Sun-facing attitude [19,20,21]. The SD option is applied to the noteworthy case of polar orbits around Venus and with an apoapsis above the North pole of the planet [22]. Venus is indeed an effective scenario where to apply the SD concept for generating artificial heliosynchronous orbits because of two significant properties: 1) the negligible eccentricity of its orbit, approximately equal to 0.0068 only, and 2) the small axial tilt of the planet, which is inclined of about 2.64 deg and has a retrograde rotation. In this situation, when the SD orbit is perpendicular to the Sun-Venus line, a simple on-off control law is sufficient to generate quasi-frozen heliosynchronous orbits.

In such a simplified model, the SD is merely subjected to the gravitational field of Venus (all of the zonal harmonics being neglected) and to the propulsive acceleration a_N due to the solar radiation pressure, which acts perpendicular to the SD orbital plane. The derivatives of the spacecraft orbital parameters $\{a, e, i, \omega, \Omega\}$ with

respect to the true anomaly ν are [23]

$$\frac{\mathrm{d}a}{\mathrm{d}\nu} = \frac{\mathrm{d}e}{\mathrm{d}\nu} = 0 \tag{1}$$

$$\frac{\mathrm{d}i}{\mathrm{d}\nu} = \frac{p^2}{\mu_{\mathrm{♀}}} \frac{\cos(\nu+\omega)}{(1+e\,\cos\nu)^3}\, a_N \tag{2}$$

$$\frac{\mathrm{d}\omega}{\mathrm{d}\nu} = \frac{p^2}{\mu_{\mathrm{♀}}} \frac{-\sin(\nu+\omega)}{(1+e\,\cos\nu)^3\,\tan i}\, a_N \tag{3}$$

$$\frac{\mathrm{d}\Omega}{\mathrm{d}\nu} = \frac{p^2}{\mu_{\mathrm{♀}}} \frac{\sin(\nu+\omega)}{(1+e\,\cos\nu)^3\,\sin i}\, a_N \tag{4}$$

where $\{a,\, e,\, i,\, \omega,\, \Omega\}$ are the osculating semimajor axis, eccentricity, inclination, argument of periapsis, and right ascension of the ascending node, respectively. In Eqs. (2)–(4), $p \triangleq a\,(1-e^2)$ is the (constant) semilatus rectum of the SD orbit, whereas $\mu_{\mathrm{♀}} = 1\,\mathrm{DU}_{\mathrm{♀}}^3/\mathrm{TU}_{\mathrm{♀}}^2$ is the gravitational parameter of Venus, where $1\,\mathrm{DU}_{\mathrm{♀}} \equiv R_{\mathrm{♀}} \simeq 6051.8\,\mathrm{km}$ is the mean radius of Venus, and $1\,\mathrm{TU}_{\mathrm{♀}} \simeq 826\,\mathrm{s}$. The propulsive acceleration a_N provided by a SD is proportional to the lightness number $\beta = \{\beta_{\min};\, \beta_{\max}\}$, which is a performance parameter defined as the ratio of the maximum acceleration due to solar radiation pressure to the gravitational attraction of the Sun at a given heliocentric distance [24]. Therefore, a_N may be written as

$$a_N = \beta\, \frac{\mu_{\odot}}{a_{\mathrm{♀}}^2} \tag{5}$$

where $\mu_{\odot} \simeq 4.0853 \times 10^5\,\mathrm{DU}_{\mathrm{♀}}^3/\mathrm{TU}_{\mathrm{♀}}^2$ is the gravitational parameter of the Sun, and $a_{\mathrm{♀}} \simeq 1.7880 \times 10^8\,\mathrm{DU}_{\mathrm{♀}}$ is the semimajor axis of Venus' orbit. Note that, due to the small eccentricity of Venus' orbit, the Sun-SD distance is always approximately equal to $a_{\mathrm{♀}}$.

2.1. Control law

With reference to Eq. (2), the requirement that the periodical variation of i is equal to zero may be formalized in mathematical terms as

$$\int_{-\omega}^{-\omega+2\pi} \frac{\cos(\nu+\omega)}{(1+e\,\cos\nu)^3}\, a_N\, \mathrm{d}\nu = 0 \tag{6}$$

from which it may be expected that $i(\nu) \simeq i_0 \triangleq \pi/2\,\mathrm{rad}\ \forall\nu$ (where the subscript 0 denotes the initial reference value). In that case, the argument of periapsis is also constant as $\mathrm{d}\omega/\mathrm{d}\nu \simeq 0$ when $i \simeq \pi/2\,\mathrm{rad}$; see Eq. (3). Therefore, it is possible to approximate ω with its initial value, that is, $\omega(\nu) \simeq \omega_0 \triangleq 3\,\pi/2\,\mathrm{rad}\ \forall\nu$. In fact, recall that the SD option is here applied to the noteworthy case of polar orbit around Venus, with its apoapsis above the North pole of the planet, as is schematically illustrated in Fig. 1.

Actually, ω will slightly change because Eq. (6) only ensures that $i \equiv i_0$ after one revolution of the SD around Venus. Moreover, the perturbative accelerations acting on the SD orbital plane may theoretically produce a drift of the apse line. Such perturbative sources, however, are not taken into account in the evaluation of the analytical control law. When $\omega \simeq \omega_0$, Eq. (6) may be equivalently rewritten as

$$\int_{-3\,\pi/2}^{\pi/2} \frac{\sin\nu}{(1+e\,\cos\nu)^3}\, a_N\, \mathrm{d}\nu = 0 \tag{7}$$

Note that the extremes of integration $\nu = -3\,\pi/2\,\mathrm{rad}$ and $\nu = \pi/2\,\mathrm{rad}$ correspond to the ascending node of the SD orbit; see Fig. 1.

Consider now Eq. (4). When $i \simeq i_0\,\mathrm{rad}$ (that is, when $\sin i \simeq 1$) and $\omega \simeq \omega_0$, the heliosynchronous condition can be written as

$$\int_{-3\,\pi/2}^{\pi/2} -\frac{\cos\nu}{(1+e\,\cos\nu)^3}\, a_N\, \mathrm{d}\nu = \frac{\mu_{\mathrm{♀}}}{p^2}\left(T\,\omega_{\mathrm{♀}}\right) = \frac{2\,\pi\,\omega_{\mathrm{♀}}}{(1-e^2)^2}\,\sqrt{\frac{\mu_{\mathrm{♀}}}{a}} \tag{8}$$

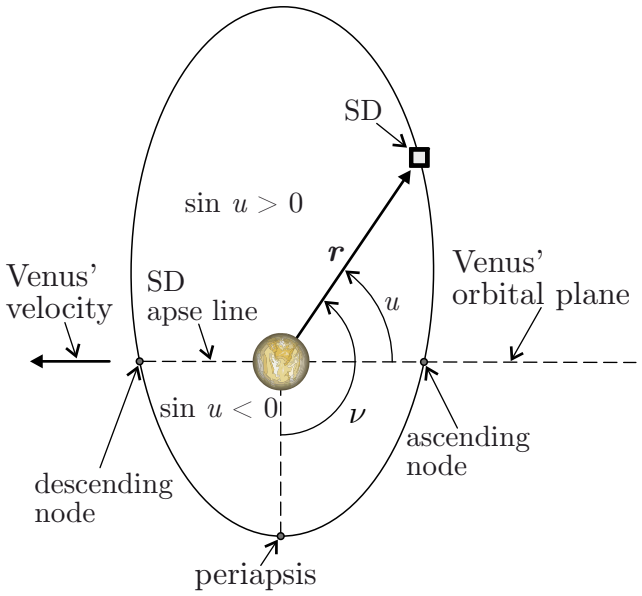

Fig. 1 Schematic representation of SD orbit.

where $T \triangleq 2\pi\sqrt{a^3/\mu_{\varnothing}}$ is the orbital period of the spacecraft, while $\omega_{\varnothing} \triangleq \sqrt{\mu_{\odot}/a_{\varnothing}^3} \simeq 2.6733 \times 10^{-4}\,\mathrm{rad/TU_{\varnothing}}$ is the mean motion of the planet. Note that $\left(T\,\omega_{\varnothing}\right)$ is the angle swept out by the planet throughout T.

Equations (7) and (8) are the two requirements that have to be satisfied in order to create heliosynchronous Taranis orbits by suitably changing the value of the lightness number β. To that end, the assumption is made that the value of β switches when the SD crosses the line of nodes. In fact, in order to increase the right ascension of the ascending node, it is useful to maximize a_N when $\mathrm{sign}\,(\sin u) > 0$ and, conversely, to minimize it when $\mathrm{sign}\,(\sin u) < 0$. To that end, consider the design parameter $n \triangleq \beta_{\max}/\beta_{\min} > 1$, defined as the (constant) ratio of the maximum to the minimum propulsive acceleration provided by a SD at a given heliocentric distance. With the previous assumptions, the lightness number may be written as

$$\beta = \frac{\beta_{\min}}{2}\,\left[n + 1 + (n-1)\,\mathrm{sign}\,(\sin u)\right] \tag{9}$$

where $u \triangleq \nu + \omega$ is the argument of latitude. Therefore, for a given value of n, a_N is a function of the spacecraft position through the argument of latitude u, and is proportional to $\beta_{\min}$, which must be determined in order to satisfy Eqs. (7) and (8). To that end, introduce the functions f and g defined as

$$f \triangleq \frac{\sin\nu}{(1+e\,\cos\nu)^3} \quad , \quad g \triangleq -\frac{\cos\nu}{(1+e\,\cos\nu)^3} \tag{10}$$

and assume F and G to be the their primitives, that is

$$F \triangleq \int \frac{\sin\nu}{(1+e\,\cos\nu)^3}\,\mathrm{d}\nu \quad , \quad G \triangleq \int -\frac{\cos\nu}{(1+e\,\cos\nu)^3}\,\mathrm{d}\nu \tag{11}$$

It may be verified that

$$F = \frac{1}{2\,e\,(1+e\,\cos\nu)^2} \tag{12}$$

$$G = \frac{3\,e\,\left\{\arctan\left[\sqrt{\dfrac{1-e}{1+e}}\,\tan\left(\dfrac{\nu}{2}\right)\right] + \dfrac{\nu}{2} - \arctan\left[\tan\left(\dfrac{\nu}{2}\right)\right]\right\}}{(1-e^2)^{5/2}} - \frac{\sin\nu\,\left[\left(e+2\,e^3\right)\cos\nu + e^2 + 2\right]}{2\,\left(1-e^2\right)^2\,(1+e\,\cos\nu)^2} \tag{13}$$

With the control law defined by Eq. (9), and taking Eq. (12) into account, it may be checked that Eq. (7) is automatically met. Instead, Eq. (8) implies

$$\beta_{\min} = \frac{2\,\pi\,\sqrt{\mu_{\varsigma}/\mu_{\odot}}\,\sqrt{a_{\varsigma}/a}\,\sqrt{1-e^2}}{(n-1)\left[(2+e^2)\,\sqrt{1-e^2} - 6\,e\,\arctan\left(\sqrt{\frac{1-e}{1+e}}\right)\right] + 3\,\pi\,n\,e} \tag{14}$$

Therefore, an increase of n reduces the required $\beta_{\min}$. Moreover, $\beta_{\min}$ is inversely proportional to $\sqrt{a}$, and is a monotonic decreasing function of e. In particular, the maximum value of $\beta_{\min}$ relative to e is

$$\beta_{\min}(e=0) = \frac{\pi\,\sqrt{\mu_{\varsigma}/\mu_{\odot}}\,\sqrt{a_{\varsigma}/a}}{n-1} \tag{15}$$

whereas $\beta_{\min}$ tends to zero when $e \to 1^{-}$. However, the maximum allowable value of e (that is, $e_{\max}$) is related to the spacecraft semimajor axis a and to the periapsis altitude (that is, $h_{\min}$) of the SD orbit as

$$e_{\max} = 1 - \frac{R_{\varsigma} + h_{\min}}{a} \tag{16}$$

3. Case study

The procedure discussed in the previous section is here applied to three particular SD configurations (referred to as SD_1, SD_2, and SD_3), of which the characteristics are taken from Refs. [25,21] and are reported in Tab. 1.

Table 1 SD characteristics. Data taken from Refs. [25,21].

SD	$\beta_{\max}$	$\beta_{\min}$	n
SD_1	0.0241	0.0134	1.8
SD_2	0.0451	0.0251	1.8
SD_3	0.0756	0.0420	1.8

In these three cases $n = 1.8$, therefore the required $\beta_{\min}$ may be written as a function of a and e as

$$\beta_{\min} = \frac{10\,\pi\,\sqrt{\mu_{\varsigma}/\mu_{\odot}}\,\sqrt{a_{\varsigma}/a}\,\sqrt{1-e^2}}{4\left[(2+e^2)\,\sqrt{1-e^2} - 6\,e\,\arctan\left(\sqrt{\frac{1-e}{1+e}}\right)\right] + 27\,\pi\,e} \tag{17}$$

It is useful to obtain a relationship that, for given values of $\beta_{\min}$ and e, provides the (unique) feasible value of a. To that end, consider Eq. (17) and introduce the function $\gamma(e)$ defined as

$$\gamma(e) \triangleq \frac{100\,\pi^2\left(1-e^2\right)}{\left\{4\left[(2+e^2)\,\sqrt{1-e^2} - 6\,e\,\arctan\left(\sqrt{\frac{1-e}{1+e}}\right)\right] + 27\,\pi\,e\right\}^2} \tag{18}$$

such that

$$a = \frac{\mu_{\varsigma}}{\mu_{\odot}}\,\frac{a_{\varsigma}\,\gamma(e)}{\beta_{\min}^2} \tag{19}$$

Figure 2 shows that $\gamma(e)$ is a decreasing function of $e \in [0,\,1)$. Therefore, for a given value of $\beta_{\min}$, the feasible minimum semimajor axis is obtained when $e = e_{\max}$; see Eq (16).

The orbital parameters of the feasible working orbits around Venus are shown in Fig. 3 when $h_{\min} \triangleq 250\,\text{km}$, which corresponds to the thickness of Venus' atmosphere [11]. Figure 3 also shows the envelope curve that delimits the region of acceptable orbits ($r_p \geq r_{\min}$) from that of ineligible ones ($r_p < r_{\min}$), being r_p the periapsis radius and $r_{\min} \triangleq h_{\min} + R_{\varsigma}$. Note that for the SD_3 configuration the feasible minimum-energy orbit is characterized by a semimajor axis of $3.4788\,\text{DU}_{\varsigma}$ and an eccentricity equal to 0.7007.

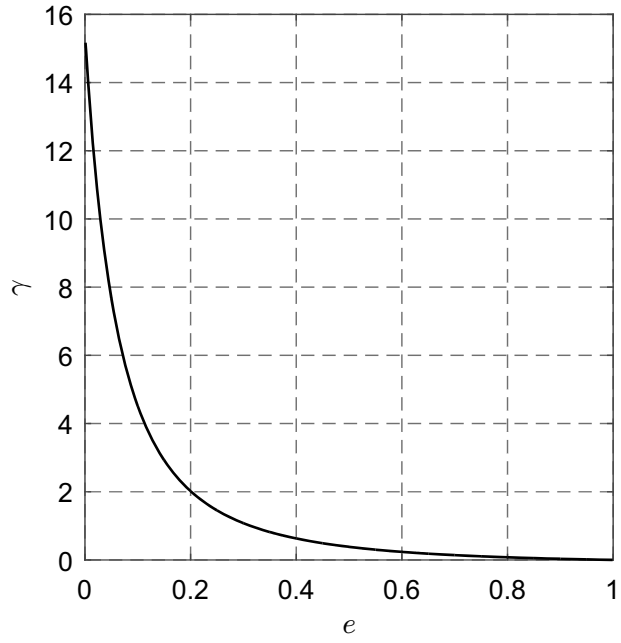

Fig. 2 γ as a function of e.

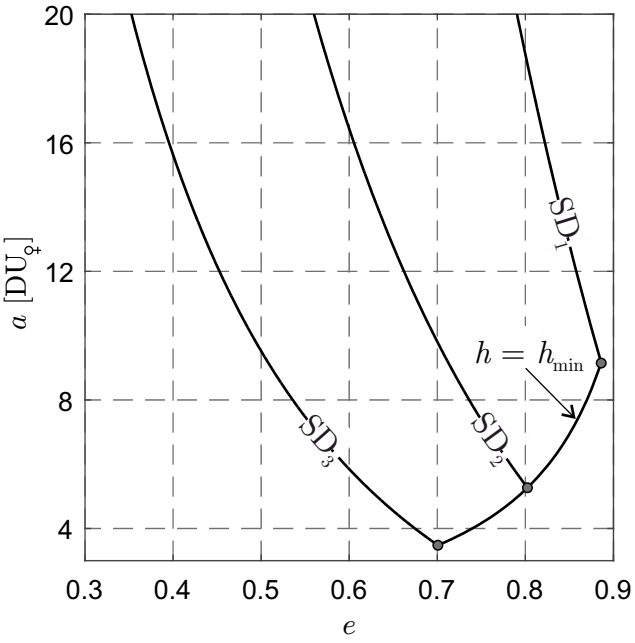

Fig. 3 Variation of a with e with $h_{\min} \triangleq 250\,\text{km}$.

3.1. Numerical simulations

The control law is validated through numerical integration of the equations of motion with the addition of the orbital perturbations. In the simulations it is assumed that the total force acting on the Smart Dust is given by three contributions: the solar radiation pressure, the third-body perturbation due to the Sun, and the gravitational field of Venus up to the J_4 zonal harmonic. In fact, the zonal harmonics $J_2 = 4.458 \times 10^{-6}$, $J_3 = -2.1082 \times 10^{-6}$, and $J_4 = -2.1471 \times 10^{-6}$ of Venus are of the same order of magnitude [22, 11], hence, they are all included in the numerical simulations. Let $\boldsymbol{r}$ be the position vector of the SD with respect to the center of mass of Venus, then the vectorial equation of motion is

$$\ddot{\boldsymbol{r}} = \boldsymbol{a}_\odot + \boldsymbol{a}_\varphi \tag{20}$$

where

$$\boldsymbol{a}_{\odot} \triangleq \mu_{\odot} \left\{ \frac{\boldsymbol{r} - \boldsymbol{r}_{\odot}}{\|\boldsymbol{r} - \boldsymbol{r}_{\odot}\|^3} \; (\beta - 1) \; \frac{\boldsymbol{r}_{\odot}}{\|\boldsymbol{r}_{\odot}\|^3} \right\} \tag{21}$$

$$\boldsymbol{a}_{\varphi} \triangleq \nabla \left\{ \frac{\mu_{\varphi}}{\|\boldsymbol{r}\|} \left[1 - \sum_{n=2}^{4} J_n \left(\frac{R_{\varphi}}{\|\boldsymbol{r}\|} \right)^n P_n \left(\frac{z}{\|\boldsymbol{r}\|} \right) \right] \right\} \tag{22}$$

are the acceleration vectors due to Sun and Venus, respectively, in which z represents the distance of the SD from the equatorial plane of the planet, whereas the lightness number β is given by Eq. (9) and (17). In particular, for $n = 1.8$, β becomes

$$\beta = \frac{2\,\pi \, \sqrt{\mu_{\varphi}/\mu_{\odot}} \, \sqrt{a_{\varphi}/a_0} \, \sqrt{1 - e_0^2} \, [7 - 2\,\mathrm{sign}\,(\cos \nu)]}{4 \left[\left(2 + e_0^2\right) \, \sqrt{1 - e_0^2} - 6\, e_0 \, \arctan\left(\sqrt{\frac{1 - e_0}{1 + e_0}} \right) \right] + 27\,\pi\, e_0} \tag{23}$$

where the subscript 0 denotes the (reference) initial value. Also, $\boldsymbol{r}_{\odot}$ is the position of the Sun with respect to Venus (see Fig. 4), which is taken from the JPL ephemeris for the time window between the 1$^{\mathrm{st}}$ of January 2019 to the 1$^{\mathrm{st}}$ of January 2029 [1]. Finally, $P_n(x)$ is the Legendre polynomial of degree n, defined as

$$P_n(x) \triangleq \frac{1}{2^n \, n!} \, \frac{\mathrm{d}^n}{\mathrm{d}x^n} \left[\left(x^2 - 1\right)^n \right] \tag{24}$$

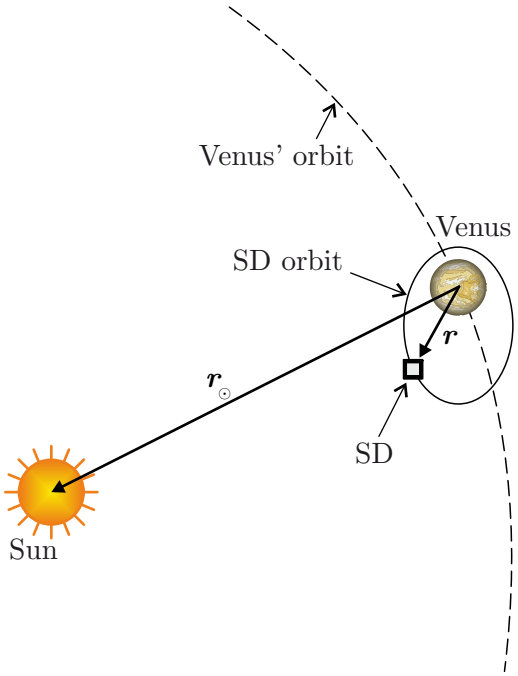

Fig. 4 Schematic representation of $\boldsymbol{r}$ and $\boldsymbol{r}_{\odot}$ vectors.

The time evolution of the orbital parameters $\{a,\, e,\, i,\, \omega,\, \Omega\}$, under the influence of the solar radiation pressure, the perturbative acceleration due to the J_2, J_3, and J_4 zonal harmonics of Venus, and the third-body perturbation due to the Sun is investigated in order to confirm the soundness of the analytical control law described by Eq. (23). The orbital parameters of the initial orbit are chosen consistently with those of the scenario described by Anderson et al. [22], who selected $a_0 = 4.1072\,\mathrm{DU}_{\varphi}$ (i.e., $T_0 = 12$ hours), $e_0 = 0.7244$, and $\omega_0 = 270$ deg. Assuming a SD_3

[1] Data retrieved from `https://ssd.jpl.nasa.gov/?planet_eph_export`

configuration (see Tab. 1), $a_0 = 4.1072\,\mathrm{DU}_{\varphi}$ implies $e_0 = 0.6696$ (see Fig. 3), which slightly differs from the case study of Ref. [22].

The simulation runs starting from JD = 2458545.53 UTC, which corresponds to the first equinox of Venus after 1st January 2019. In that date, the angle α between the Sun-Venus line and the orbital plane of the SD is zero if $\Omega_0 = 328.83$ deg. Figure 5 shows that the previously discussed control law (see Fig. 6) is actually able to meet the heliosynchronous condition. The fluctuations of orbital inclination and argument of periapsis (see Figs. 7 and 8) are on the order of a few degrees, while the semimajor axis and the eccentricity vary less than 0.09% and 0.48%, respectively, with respect to their nominal values, as shown in Figs. 9 and 10. In fact, Fig. 11 shows that α fluctuates between 0 and 2.11 deg during the three year-long simulation, consistently with the small axial tilt of Venus. Such an angle yields a disturbance acceleration on the SD orbital plane, which causes the aforesaid fluctuations of a and e, and, also, a drift of the apse line. However, those fluctuations are an acceptable cost, as the heliosynchronous condition is exactly met with a simple control law to implement, and, moreover, the attitude control is performed in a totally passive way.

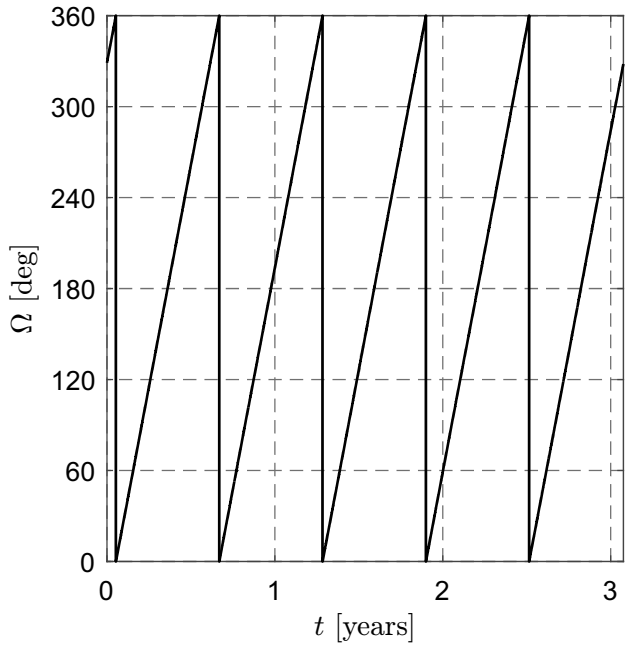

Fig. 5 Variation of Ω in the SD_3 case for $T = 12$ hours.

4. Conclusions

This paper has investigated the generation of heliosynchronous Taranis orbits around Venus. It has been shown that such a goal may be achieved using the Smart Dust concept, which can provide two levels of propulsive acceleration thanks to the coverage of its surface with electrochromic material. A simple on-off control law has been obtained in closed form as a function of the characteristics of the Smart Dust working orbit. A numerical integration of the Smart Dust equations of motion has proved the soundness of the analytical control law by also including some perturbative sources in the simulation code.

References

1. Anderson, P. and Macdonald, M., "Sun-synchronous highly elliptical orbits using low-thrust propulsion," *Journal of Guidance, Control, and Dynamics*, Vol. 36, No. 6, November-December 2013, pp. 1849–1855. doi: 10.2514/1.59848.
2. Hanson, J. N. and Fairweather, S. H., "Nodal rotation for continuous exposure of an Earth satellite to the Sun," *ARS Journal*, Vol. 31, No. 5, May 1961, pp. 640–645. doi: 10.2514/8.5587.
3. Macdonald, M., McKay, R., Vasile, M., et al., "Extension of the Sun-synchronous orbit," *Journal of Guidance, Control, and Dynamics*, Vol. 33, No. 6, November-December 2010, pp. 1935–1939. doi: 10.2514/1.49011.

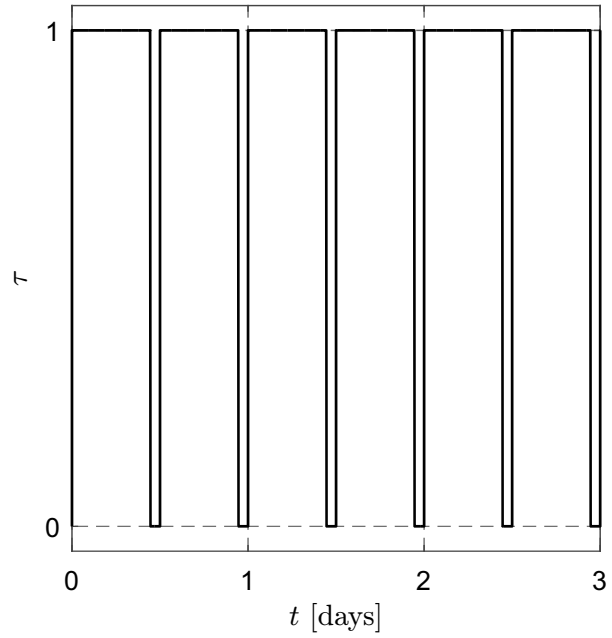

Fig. 6 SD_3 control law.

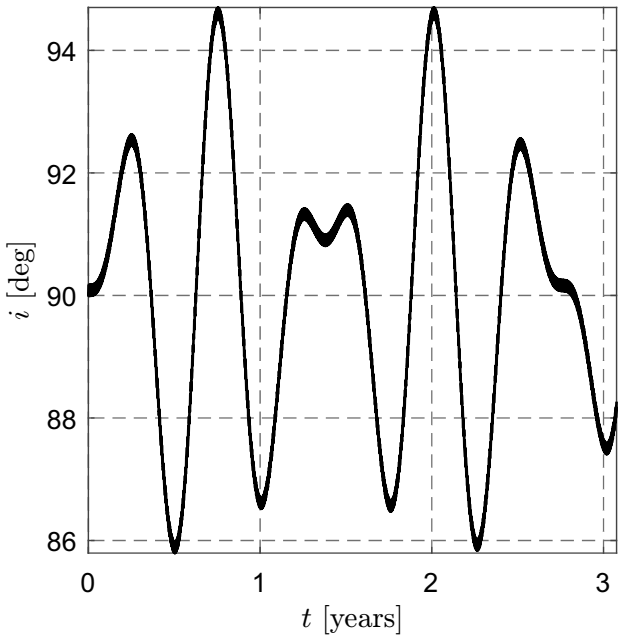

Fig. 7 Variation of i in the SD_3 case for $T = 12$ hours..

4. Docherty, S. Y. and Macdonald, M., "Analytical Sun-synchronous low-thrust orbit maneuvers," *Journal of Guidance, Control, and Dynamics*, Vol. 35, No. 2, March-April 2012, pp. 681–686. doi: 10.2514/1.54948.
5. Wu, Z., Jiang, F., and Li, J., "Extension of frozen orbits and Sun-synchronous orbits around terrestrial planets using continuous low-thrust propulsion," *Astrophysics and Space Science*, Vol. 360, No. 1, November 2015, pp. 1–16. doi: 10.1007/s10509-015-2529-7.
6. Kahn, J. M., Katz, R. H., and Pister, K. S. J., "Next century challenges: mobile networking for "Smart Dust"," *5th ACM/IEEE International Conference on Mobile and Computing Networks*, Seattle, WA, USA, August 1999, pp. 271–278.
7. Niccolai, L., Bassetto, M., Quarta, A. A., and Mengali, G., "A review of Smart Dust architecture, dynamics, and mission applications," *Progress in Aerospace Sciences*, Vol. 106, April 2019, pp. 1–14. doi: 10.1016/j.paerosci.2019.01.003.
8. Atchison, J. A. and Peck, M. A., "Length scaling in spacecraft dynamics," *Journal of Guidance, Control, and Dynamics*, Vol. 34, No. 1, January-February 2011, pp. 231–246. doi: 10.2514/1.49383.
9. Tscherbakova, N. N., Beletskii, V. V., and Sazonov, V. V., "Stabilization of heliosynchronous orbits of an Earth's artificial satellite by solar pressure," *Cosmic Research*, Vol. 37, No. 4, 1999, pp. 417–427.

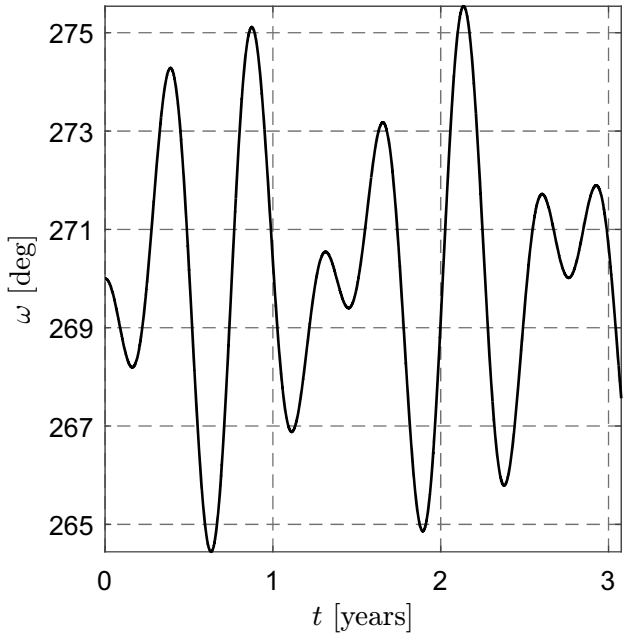

Fig. 8 Variation of ω in the SD_3 case for $T = 12$ hours..

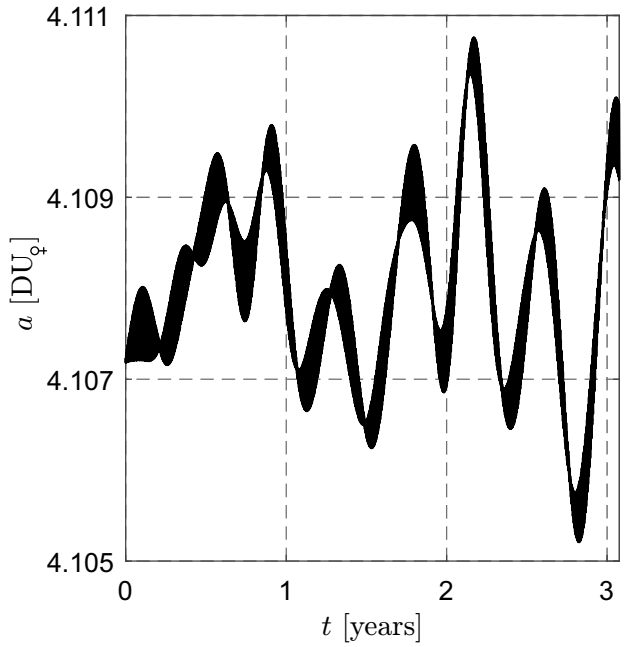

Fig. 9 Variation of a in the SD_3 case for $T = 12$ hours..

10. Cao, J., Clemente, C., McInnes, C., et al., "A novel concept for Earth remote sensing using a bi-static femto-satellite swarm in Sun-synchronous orbit," *Proceedings of the International Astronautical Congress, IAC*, Vol. 6, 2015, pp. 4654–4662.
11. De Oliveira, M. R. R., Gil, P. J. S., and Ghail, R., "A novel orbiter mission concept for Venus with the EnVision proposal," *Acta Astronautica*, Vol. 148, July 2018, pp. 260–267. doi: 10.1016/j.actaastro.2018.05.012.
12. Macdonald, M., Anderson, P., and Warren, C., "A novel design concept for space-based polar remote sensing," *Proceedings of SPIE*, Vol. 8533, November 2012.
13. Anderson, P. and Macdonald, M., "Extension of highly elliptical Earth orbits using continuous low-thrust propulsion," *Journal of Guidance, Control, and Dynamics*, Vol. 36, No. 1, January-February 2013, pp. 282–292. doi: 10.2514/1.55304.
14. Anderson, P. and Macdonald, M., "Static, highly elliptical orbits using hybrid low-thrust propulsion," *Journal of Guidance, Control, and Dynamics*, Vol. 36, No. 3, May-June 2013, pp. 870–880. doi: 10.2514/1.56636.
15. Monk, P. M. S., Mortimer, R. J., and Rosseinsky, D. R., *Electrochromism: Fundamentals and Applications*, Wiley-VCH, 2007.

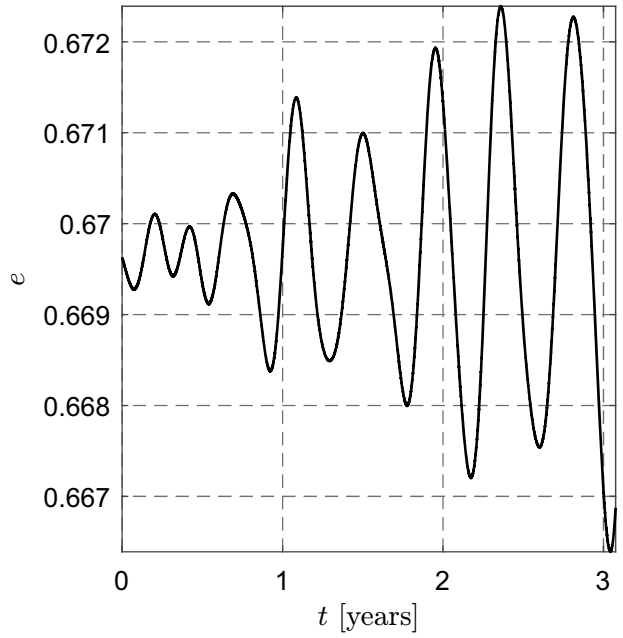

Fig. 10 Variation of e in the SD_3 case for $T = 12$ hours..

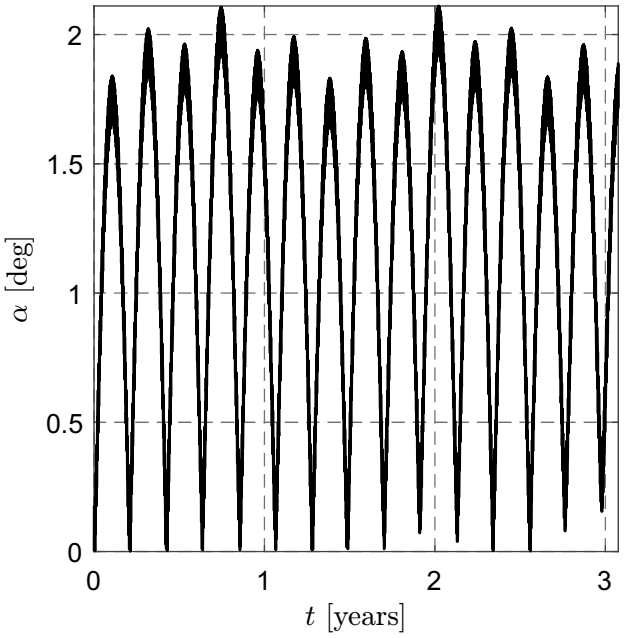

Fig. 11 Variation of α in the SD_3 case for $T = 12$ hours..

16. Lücking, C., Colombo, C., and McInnes, C. R., "Orbit control of high area-to-mass ratio spacecraft using electrochromic coating," *61st International Astronautical Congress (IAC)*, Prague, Czech Republic, September-October 2010, pp. 1923–1937.
17. Lücking, C., Colombo, C., and McInnes, C. R., "Electrochromic orbit control for Smart Dust devices," *Journal of Guidance, Control, and Dynamics*, Vol. 35, No. 5, September 2012, pp. 1548–1558. doi: 10.2514/1.55488.
18. Colombo, C., Lücking, C., and McInnes, C. R., "Orbit evolution, maintenance and disposal of SpaceChip swarms through electro-chromic control," *Acta Astronautica*, Vol. 82, No. 1, January 2013, pp. 25–37. doi: 10.1016/j.actaastro.2012.05.035.
19. Atchison, J. A. and Peck, M. A., "A passive, Sun-pointing, millimeter-scale solar sail," *Acta Astronautica*, Vol. 67, No. 1–2, July 2010, pp. 108–121. doi: 10.1016/j.actaastro.2009.12.008.
20. Mengali, G. and Quarta, A. A., "Heliocentric trajectory analysis of Sun-pointing Smart Dust with electrochromic control," *Advances in Space Research*, Vol. 57, No. 4, February 2016, pp. 991–1001. doi: 10.1016/j.asr.2015.12.017.
21. Mengali, G., Quarta, A. A., and Denti, E., "Relative motion of Sun-pointing Smart Dust in circular heliocentric orbits," *Journal of Guidance, Control, and Dynamics*, Vol. 41, No. 4, April 2018, pp. 1009–1014. doi: 10.2514/1.G003088.

22. Anderson, P., Macdonald, M., and Yen, C., "Novel orbits of Mercury, Venus and Mars enabled using low-thrust propulsion," *Acta Astronautica*, Vol. 94, No. 2, February 2014, pp. 634–645. doi: 10.1016/j.actaastro.2013.08.018.
23. Battin, R. H., *An Introduction to the Mathematics and Methods of Astrodynamics, Revised Edition*, AIAA, Reston, Virginia, 1999.
24. McInnes, C. R., *Solar Sailing: Technology, Dynamics and Mission Applications*, Springer-Verlag, 1999.
25. Colombo, C. and McInnes, C. R., "Orbital dynamics of Smart Dust devices with solar radiation pressure and drag," *Journal of Guidance, Control, and Dynamics*, Vol. 34, No. 6, 2011, pp. 1613–1631. doi: 10.2514/1.52140.